

# Automated motion estimation of root responses to sucrose in two *Arabidopsis thaliana* genotypes using confocal microscopy

Nathalie Wuyts · A. Glyn Bengough · Timothy J. Roberts ·  
Chengjin Du · M. Fraser Bransby · Stephen J. McKenna ·  
Tracy A. Valentine

Received: 15 December 2010 / Accepted: 8 May 2011  
© Springer-Verlag 2011

**Abstract** Root growth is a highly dynamic process influenced by genetic background and environment. This paper reports the development of *R* scripts that enable root growth kinematic analysis that complements a new motion analysis tool: *PlantVis*. Root growth of *Arabidopsis thaliana* expressing a plasma membrane targeted GFP (C24 and Columbia 35S:LT16b-EGFP) was imaged using time-lapse confocal laser scanning microscopy. Displacement of individual pixels in the time-lapse sequences was estimated automatically by *PlantVis*, producing dense motion vector fields. *R* scripts were developed to extract kinematic growth parameters and report displacement to  $\pm 0.1$  pixel. In contrast to other currently available tools, *Plantvis-R* delivered root velocity profiles without interpolation or averaging across the root surface and also estimated the uncertainty associated with tracking each pixel. The

*PlantVis-R* analysis tool has a range of potential applications in root physiology and gene expression studies, including linking motion to specific cell boundaries and analysis of curvature. The potential for quantifying genotype  $\times$  environment interactions was examined by applying *PlantVis-R* in a kinematic analysis of root growth of C24 and Columbia, under contrasting carbon supply. Large genotype-dependent effects of sucrose were recorded. C24 exhibited negligible differences in elongation zone length and elongation rate but doubled the density of lateral roots in the presence of sucrose. Columbia, in contrast, increased its elongation zone length and doubled its elongation rate and the density of lateral roots.

**Keywords** Cell expansion · Confocal laser scanning microscopy · Digital image analysis · Motion estimation · Root meristem · Sucrose

**Electronic supplementary material** The online version of this article (doi:10.1007/s00425-011-1435-7) contains supplementary material, which is available to authorized users.

N. Wuyts · A. G. Bengough · T. A. Valentine (✉)  
Scottish Crop Research Institute,  
Dundee DD2 5DA, UK  
e-mail: Tracy.Valentine@scri.ac.uk

T. J. Roberts · C. Du · S. J. McKenna  
School of Computing, University of Dundee,  
Dundee DD1 4HN, UK

A. G. Bengough · M. F. Bransby  
Division of Civil Engineering, University of Dundee,  
Dundee DD1 4HN, UK

*Present Address:*

N. Wuyts  
Earth and Life Institute, Université Catholique de Louvain,  
Louvain-la-Neuve, Belgium

## Abbreviations

CLSM Confocal laser scanning microscopy  
DAG Days after germination  
DVF Displacement vector field  
EGR Elemental growth rate  
PIV Particle image velocimetry

## Introduction

The overall growth pattern of plant organs is genetically determined, but greatly influenced by environmental conditions. Cell division and expansion produce growth and the molecular and physiological processes involved are studied extensively, e.g. in roots: Beemster and Baskin

(2000); De Veylder et al. (2001); Beemster et al. (2002); Teale et al. (2005); Dello Ioio et al. (2007). Phenotypic expression of genetic variability and the impact of environmental conditions on organ or cell growth can be evaluated by growth analysis techniques that deliver high spatial and temporal resolution, i.e. that operate at the cell level (microns) and at time intervals of minutes or seconds. Live imaging technologies enable high-resolution visualisation of dynamic cellular processes, especially when combined with fluorescent marker techniques which target fluorescent signals to specific cellular compartments (Cutler et al. 2000; Kurup et al. 2005; Reddy et al. 2007) or specific stages in cell differentiation (Berger et al. 1998). Confocal laser scanning microscopy (CLSM) is particularly powerful at recording dynamic behaviour, allowing imaging at different depths (optical sectioning) over time. The large data sets obtained motivate the development of automated computational methods to extract and quantify spatio-temporal processes. Algorithms have been designed to study cell dynamics of the shoot apical meristem in *Arabidopsis thaliana*, combining in a software tool, automatic image segmentation and semi-automatic reconstruction in space and time, following CLSM image capture and pre-processing (Barbier de Reuille et al. 2005). In root growth experiments, motion analysis has evolved from manual marking and measurement to automatic processing of digital image sequences (Walter et al. 2002; van der Weele et al. 2003; Campilho et al. 2006; Basu et al. 2007; Chavarria-Krauser et al. 2008). Optical flow methods have been applied to obtain velocity fields from two-dimensional root images and to characterise motion on the outer surface of roots with resolutions from 20 microns down to 1 micron per pixel and time intervals of 2 min down to 2 s (Walter et al. 2002; van der Weele et al. 2003). Recently, particle image velocimetry (PIV), a technique developed in fluid mechanics and geotechnical engineering (White et al. 2003), has been tested for motion estimation in time-lapse CLSM image sequences of growing *A. thaliana* roots (Bengough et al. 2010). High spatial resolution was reported with PIV (<0.5 pixel) but, as in the aforementioned optical flow methods, no estimates of uncertainty are available for the individual regions that were tracked. In many of these methods, the final estimates result from extensive interpolation or averaging across the root surface or with time. An improved motion estimation tool should be flexible towards the nature of the input data (e.g. independent of the direction of motion in a two-dimensional plane) and the format of the output data. Results reported on a per pixel basis could allow motion analysis to be linked to specific tissues and cells. Recently, *PlantVis*, a new method for automated motion estimation in CSLM images, has been developed using computer vision methods and statistical modelling (Roberts et al.

2010). *PlantVis* reports on the spatio-temporal displacement of features captured by CLSM imaging, e.g. cell membranes, in a format which can be imported into statistical software, e.g. *R* (R Development Core Team 2007), for data analysis.

In this paper we have applied *PlantVis* to the study of root growth dynamics at high temporal and spatial resolution in two *A. thaliana* genotypes [C24 and Columbia (Col)]. We used the optical sectioning power of CLSM to visualise cell structure within the *Arabidopsis* root. New *R*-scripts were developed to extract and display root growth parameters such as the velocity profile along the root axis, the elemental growth rate (EGR) and the length of the division and elongation zones, enabling kinematic analysis of growth. The flexibility, utility and potential applications of *PlantVis-R* are discussed in the context of other image analysis methods including *RootflowRT* (van der Weele et al. 2003), PIV (White et al. 2003; Bengough et al. 2010), methods for measuring root growth over longer periods of time such as *RootTrace* (French et al. 2009) and measuring roots' lengths over successive days to obtain velocity measurements.

In addition, it is important that these procedures are practical for the comparison of genotypes and for the analysis of environmental effects. Exogenous sucrose is known to affect root growth (Hauser and Bauer 2000; Hermans et al. 2006; Hammond and White 2008; MacGregor et al. 2008) and it was recently shown that uptake of sucrose via the aerial tissues, when leaves are in contact with growth media, can affect both primary root growth and lateral root extension in the *A. thaliana* genotype Col (MacGregor et al. 2008). Sucrose is often a major constituent in plant growth media used in root studies of *A. thaliana* and is the major form of translocated sugar in plants, providing tissues with the hexoses required for respiration and primary and secondary metabolism. It is also a recognised signalling compound in plant development and stress (Rolland et al. 2002). It is important, therefore, to understand the influence of the presence of sucrose on root growth kinematics, and how this may vary between *A. thaliana* genotypes commonly used in experiments. We have, therefore, used this system to demonstrate the effectiveness of *PlantVis-R*, comparing the effects of sucrose on the kinematic growth processes of the two fluorescently tagged genotypes of *Arabidopsis* used in this study.

## Materials and methods

### Plant material and growth conditions

*Arabidopsis thaliana* (L.) Heyhn expressing 35S:LTI6b-EGFP (constitutively expressed *enhanced* green fluorescent

protein targeted to the plasma membrane) in the C24 and Col-0 background (Kurup et al. 2005) was used in all experiments (seeds originally sourced from Prof. J. Haseloff, University of Cambridge, UK). Surface-sterilised seeds were, unless otherwise stated, plated on 0.5× Murashige and Skoog salt mixture including vitamins, 1% sucrose and 0.7% phytoagar (Melford Laboratories Ltd, Ipswich, UK) at pH 5.8 in 9 cm diameter Petri dishes at four seeds per dish. Agar depth was less than 3 mm. After 3 days at 4°C, dishes were transferred to a growth chamber at 22°C and a 16 h light/8 h dark cycle for germination and growth (DAG = days after germination, transfer day = DAG 0). At approximately 3 DAG, dishes were placed vertically to ensure roots grew along the bottom of the dish (i.e. within the agar layer). For comparison of root responses to sucrose, plants were grown in the presence or absence of 1% sucrose.

#### Imaging of root tips and the whole root system

Imaging of growing root tips was performed using a Leica TCS SP1 confocal laser scanning upright microscope (Leica, Heidelberg, Germany, Leica Confocal Software version 2.5 Build 1347) with a 10×/0.3 (all Fig. except 6c–h) or 20×/0.5 (Fig. 6c–h) HCX APO L (water-dipping) objective lens, 488 nm excitation from an argon laser and fluorescence emission detection between 500 and 570 nm for EGFP. Plants were imaged through the underside of the Petri dishes in which they were grown without removal from the growth media to minimise disturbance of plants. Images were captured at high resolution (1,024 × 1,024 pixels, 8-bit) as time series (typically 30–120 s between frames, up to 10 frames). Imaging was of the middle of the root (root cap, epidermis, cortex, endodermis and vascular tissue distinguishable) or as a stack of sections in depth, from the surface to the middle of the root, repeated over time (typically 50 sections, acquisition time 80 s, 90 s between the beginnings of each, 10 stacks or frames). In the growing conditions described here, the complete growth zone of C24 and Col roots could be imaged in one frame (image field size of 1,000 μm). More recent confocal systems have larger image field sizes (1,500 μm). In case of larger growth zones, the motorised stage of the microscope is used to translate the root between successive time frames. In the first frame the reference is typically the quiescent centre, while a secondary reference, along the midline of the root is chosen for the second frame. Images can either be stitched (i.e. joined using the Leica Confocal Software version 2.5 Build 1347 or Leica Confocal Software Lite Version 2.61 Build 1538) before processing by *PlantVis*, or they are run separately and results are combined using the distance between the secondary reference and the quiescent centre along the root midline. To validate

the root tip velocity measurements obtained by *PlantVis* independent measurements of root tip velocity were obtained by comparing root lengths over several days. This was achieved by imaging the whole root systems using a desktop scanner (Epson Expression) at 800 dpi. These images were subsequently analysed for root length by fitting a spline in *R* through points selected manually on the root image in ImageJ (ImageJ: Rasband 2007. US National Institutes of Health, Bethesda, Maryland, USA. <http://rsb.info.nih.gov/ij>). The change in root length divided by the growth interval was used to calculate tip velocity. Lateral root number was also recorded.

#### Motion estimation in time-lapse image sequences—*PlantVis*

The *PlantVis* algorithm was implemented in Java and interfaced to ImageJ as a plugin. It is described in detail in Roberts et al. (2010). *PlantVis* automatically imports information from the metadata of Leica confocal data sets, however, images from other microscope sources can also be imported into *PlantVis* after the addition of a simple “metadata” text file to the data set folder. For a 10× image data set, motion estimation parameters typically used were as follows. Motion at each frame was estimated based on that frame, the preceding frame and the subsequent frame (i.e. three images). An upper bound on inter-frame displacement was assumed to be 8 pixels. Estimation used a circular patch of diameter 21 pixels (i.e. the software’s ‘patch size’ parameter was set to 10), and the log-likelihood threshold value was set to 80. Motion estimation data are reported as six separate image files and respective hdf files (HDF Java Products (2007) <http://hdfgroup.com/hdf-java-html>), including horizontal displacement, vertical displacement, standard deviation of horizontal displacement, standard deviation of vertical displacement, covariance of horizontal and vertical displacement and determinant of the covariance matrix of horizontal and vertical displacement. The mark-up tool in *PlantVis* was used to create text files containing the pixel coordinates of reference points, typically the quiescent centre, and points along the midline of the root or any other feature required. Motion analyses were performed on single or dual channel CLSM data sets (i.e. data sets containing simultaneously acquired images of the fluorescent LTI6b-EGFP marker and a grey scale Leica CLSM PMT transmission image visualising the laser light transmitted through the sample, see Fig. S1a).

To test the software for accuracy of motion estimation, partially artificial data sets were produced using the *Leica* microscope software: the first image was translated up (i.e. vertically) 1 or 2 pixels, and the third image in the sequence was translated down the same number of pixels. Data sets were run using the standard protocol for *PlantVis*

and the motion data output was compared with the data produced for the unaltered original data set. *PlantVis* motion estimation results were compared with motion estimates from PIV (using the fluorescent channel images; White et al. 2003; Bengough et al. 2010) and *RootflowRT* v2.8 (*RootflowRT* v2.8. 2009: Biological motion estimation for plant root growth. [http://meru.cs.missouri.edu/mvl/bio\\_motion/rootflow](http://meru.cs.missouri.edu/mvl/bio_motion/rootflow)) using the transmission CLSM channel images (van der Weele et al. 2003). Analyses were performed according to instructions provided with these tools, followed by the fitting of the step stool curve to each data set as described below.

### Data analysis and statistics

Analysis and visualisation of displacement data generated in *PlantVis* were performed using *R* (R Development Core Team. 2007: *R*: a language and environment for statistical computing. <http://www.R-project.org>). Scripts were developed that allow fast, routine calculation and display of displacement (in pixels frame<sup>-1</sup> and  $\mu\text{m min}^{-1}$ ) along the root. Longitudinal and radial velocity were calculated as the components of velocity parallel and perpendicular, respectively, to the axis of growth, defined by a cubic spline through the quiescent centre and points along the midline of the root (Fig. 1). For each data point in the root image, the distance along this spline to a reference point (typically the quiescent centre) was calculated by defining the position of the intersect with the spline of a local tangent for which the normal contains the respective data point. Distances were calculated as the arc length along the spline from the quiescent centre to the intersect (Mullen et al. 1998). The composite step-stool function of Peters and Baskin (2006) was fitted to the absolute and longitudinal velocity profiles (velocity data vs. distance from the quiescent centre) using the “nls” function in *R*. The following growth parameters were then extracted: EGR profile along the root axis, maximum EGR and its position, length of the growth zone, division zone and elongation zone, average root tip velocity and its standard deviation. In addition, a script was developed to present the direction and quantity of displacement by arrows in a ‘quiver’ plot.

Text files containing the pixel coordinates of features, e.g. tissues, cells or cell membranes, selected in *PlantVis* (point selections) or ImageJ (area selections), were used in *R* to filter results for the selected areas and distinguish them in plots.

Statistical analysis of growth rate data was performed in *R* on ten replicate outputs. Growth parameters (root length, root length increase, lateral root density, velocity, maximum EGR, position of maximum EGR, length of growth zone, division zone and elongation zone) were analysed using ANOVA (one-way or two-way). For multiple

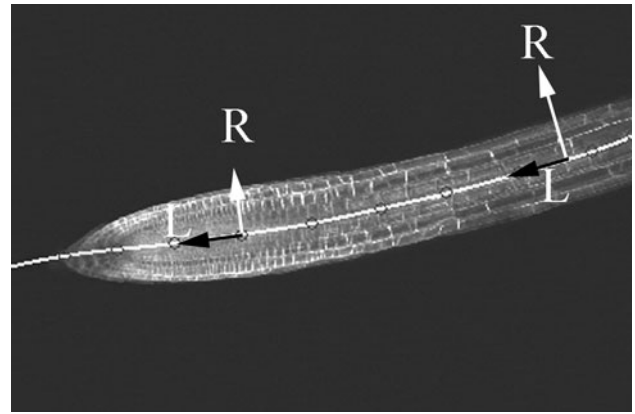


**Fig. 1** A smooth spline is fitted to the root axis and the distance from the quiescent centre for any motion estimate is the arc length along the spline from a perpendicular intersect of the position of the estimate on the axial spline. *L* longitudinal and *R* radial velocities are calculated parallel and normal to the direction of the spline at the intercept, respectively

comparisons of group means the Tukey test was applied. Pearson’s correlation coefficient was calculated to identify the extent of linear relationships between root growth parameters at an individual plant level.

### Results

Motion estimation and analysis of growth in two-dimensional CLSM time-lapse image sequences using *PlantVis-R*

*PlantVis* delivers displacement vector fields (DVF) by attempting motion estimation at every pixel location in the image. This results in no motion estimation at locations with large motion ambiguity (mostly in the background), and motion estimates at pixel locations at which motion can be estimated with relatively high certainty. Horizontal (*x*) and vertical (*y*) displacement components are reported in pixels frame<sup>-1</sup>, to the nearest 0.1 pixel frame<sup>-1</sup>. The actual spatial resolution of motion estimates depends on the image field size of the microscope system, the image resolution upon scanning and the lens magnification factor. Images were routinely captured at a resolution of  $1,024 \times 1,024$  pixels resulting in an approximate spatial resolution of  $0.1 \mu\text{m pixel}^{-1}$  and  $0.05 \mu\text{m pixel}^{-1}$  for  $10\times$  and  $20\times$  magnification, respectively. Motion estimation results for an individual *A. thaliana* C24 primary root at 8 DAG are shown in Fig. 2. They include a single image from a CLSM data set (Fig. 2a), horizontal (Fig. 2b) and vertical displacement components (Fig. 2c), and the magnitude of the displacement (Fig. 2d, see also Fig. 1). A quiver plot displays motion vectors as arrows, thereby

giving an indication of both the direction and magnitude of motion (Fig. 2e).

Motion estimates generated by *PlantVis* are further processed using *R* into velocity profiles along the root axis (Fig. 3). Figure 3a shows the central spline (green line) of the root, based on points marked up using *PlantVis*. This spline is used in the calculation of positions along the root axis relative to the quiescent centre (indicated by X). In Fig. 3b, the CLSM image (Fig. 3a) is overlaid with the motion estimate data generated by *PlantVis*. Utilising the position of the quiescent centre, the position of the spline and the frame rate, the absolute, longitudinal and radial velocities at each data point can be derived in  $\mu\text{m min}^{-1}$  (Fig. 3c, d, e respectively). A slight clustering around horizontal lines in these plots appears to be evidence of a weak pixel-locking effect (Shimizu and Okutomi 2005). The longitudinal and radial velocity profiles (Fig. 3d, e) are important parameters to consider when root growth deviates from pure uni-directional elongation (axis growth), e.g. during gravitropic responses. The radial velocity is defined as motion in a direction perpendicular to the central spline. In this data set, the root can be seen to be expanding longitudinally (Fig. 3d), but also moving radially by approximately  $0.3 \mu\text{m min}^{-1}$  (Fig. 3e). The composite step-stool function defined by Peters and Baskin (2006) was fitted to velocity profiles for the extraction of quantitative growth parameters (Fig. 3f). This function was designed to provide an independent criterion for distinguishing sigmoidal and bi-linear growth models (van der Weele et al. 2003) without forcing a dichotomous decision. A requirement of this function is the definition of zero

velocity at the reference point (position of the quiescent centre) and as such the reference frame was inverted (Fig. 3f) compared to the velocity profiles (Fig. 3d) directly derived from the experimental data. The first derivative of this function yields the EGR, for which the maximum and the position of the maximum are determined. The second derivative is used to delineate and quantify the extent of the growth zone, including the division zone and elongation zone. Although Fig. 3c–f apparently contain a wide scatter of data points, it must be noted that  $>35,000$  individual data points are represented on each graph. An examination of the residuals shows that 94% of the residuals from the step-stool curve fit are within  $\pm 0.01 \text{ mm h}^{-1}$ , thus the number of outliers is relatively small. Therefore, it must be appreciated that a large number of the points appear coincidentally when visually interpreting these plots.

Kinematic analysis: examination of *PlantVis* functions and comparison of *PlantVis-R*, PIV and *RootflowRT*

To assess the accuracy of *PlantVis* motion estimation, Roberts et al. (2010) compared the motion estimates of *PlantVis* to those calculated from manual markup of the images. The regression line produced by the comparison deviated by less than 1 standard error ( $SE = 0.077$ ) from a gradient of 1. Here we further tested the accuracy using two artificial data sets that had motion artificially increased in the vertical direction by 1 or 2 pixels per frame using the Leica confocal software. The motion estimates obtained from *PlantVis* were compared with the output from the

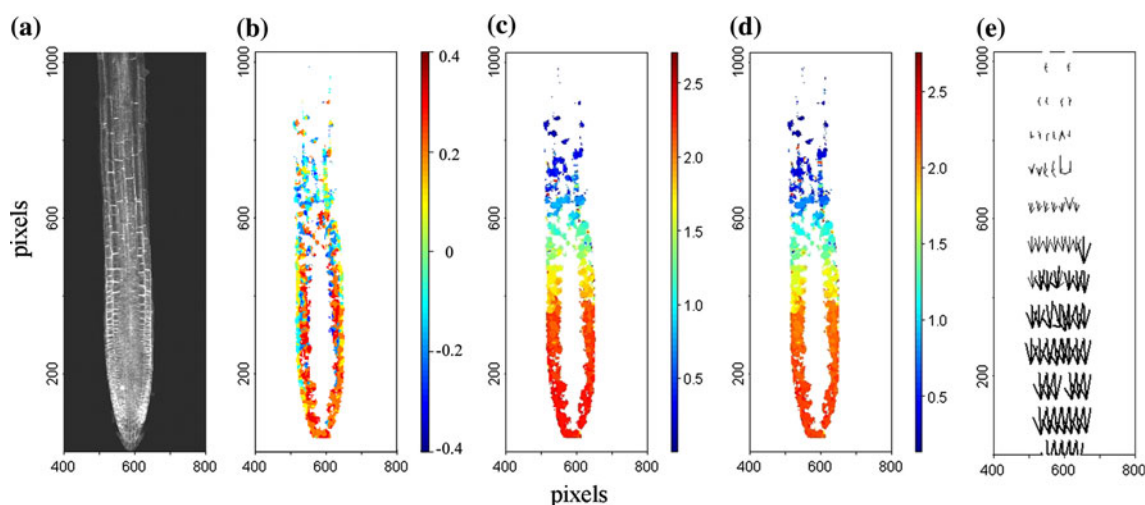
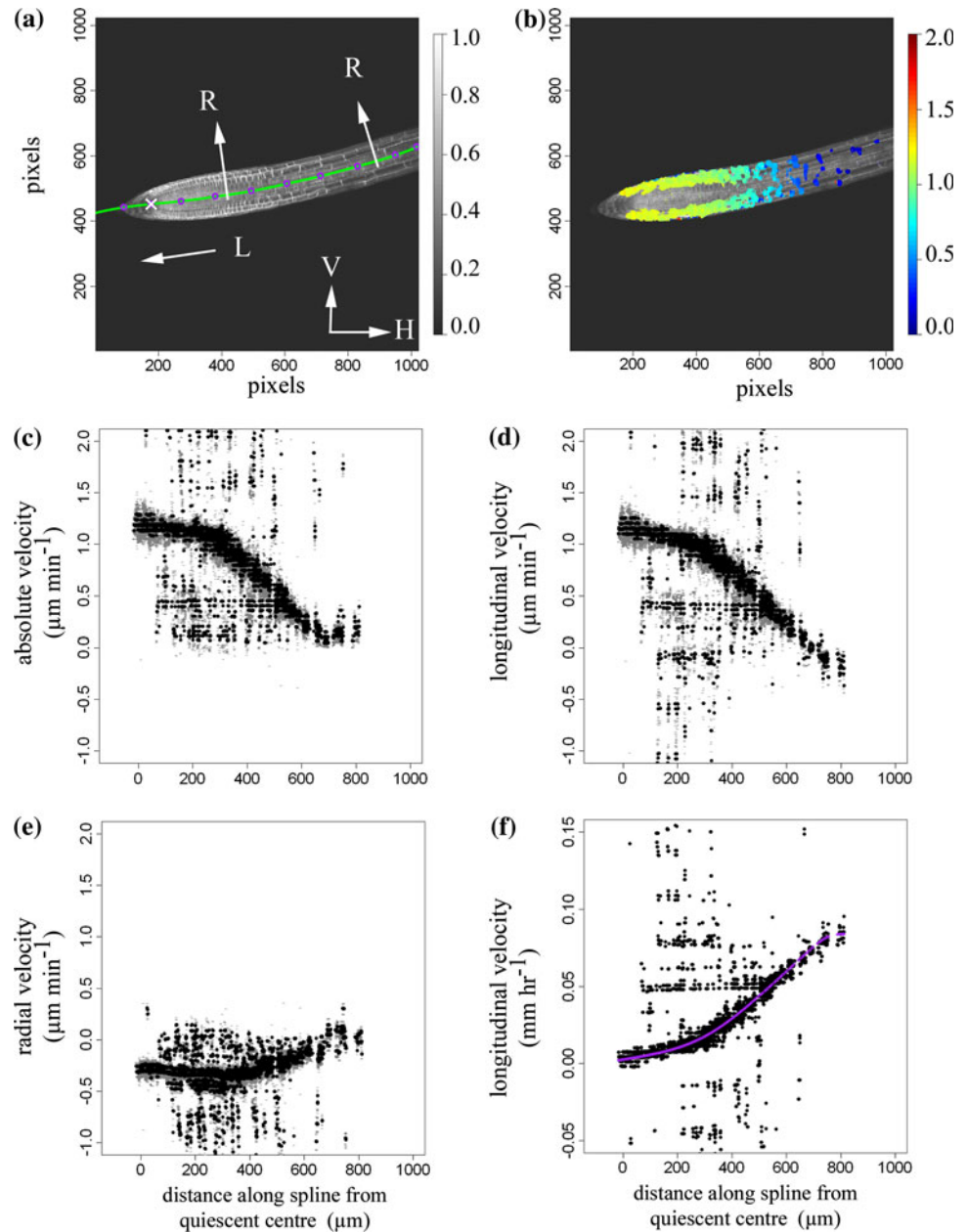


**Fig. 2** Motion estimation in a CLSM time-lapse image sequence of an *A. thaliana* C24 LTI6b-EGFP primary root (8 DAG) at  $\times 10$  magnification. **a** Confocal image. **b** Horizontal displacement (pixels frame $^{-1}$ ). **c** Vertical displacement (pixels frame $^{-1}$ ). **d** Absolute

velocity ( $\mu\text{m min}^{-1}$ ). **e** Quiver plot. Arrows represent the direction of motion, with lengths proportional to the magnitude of motion. Axis scale (pixels)

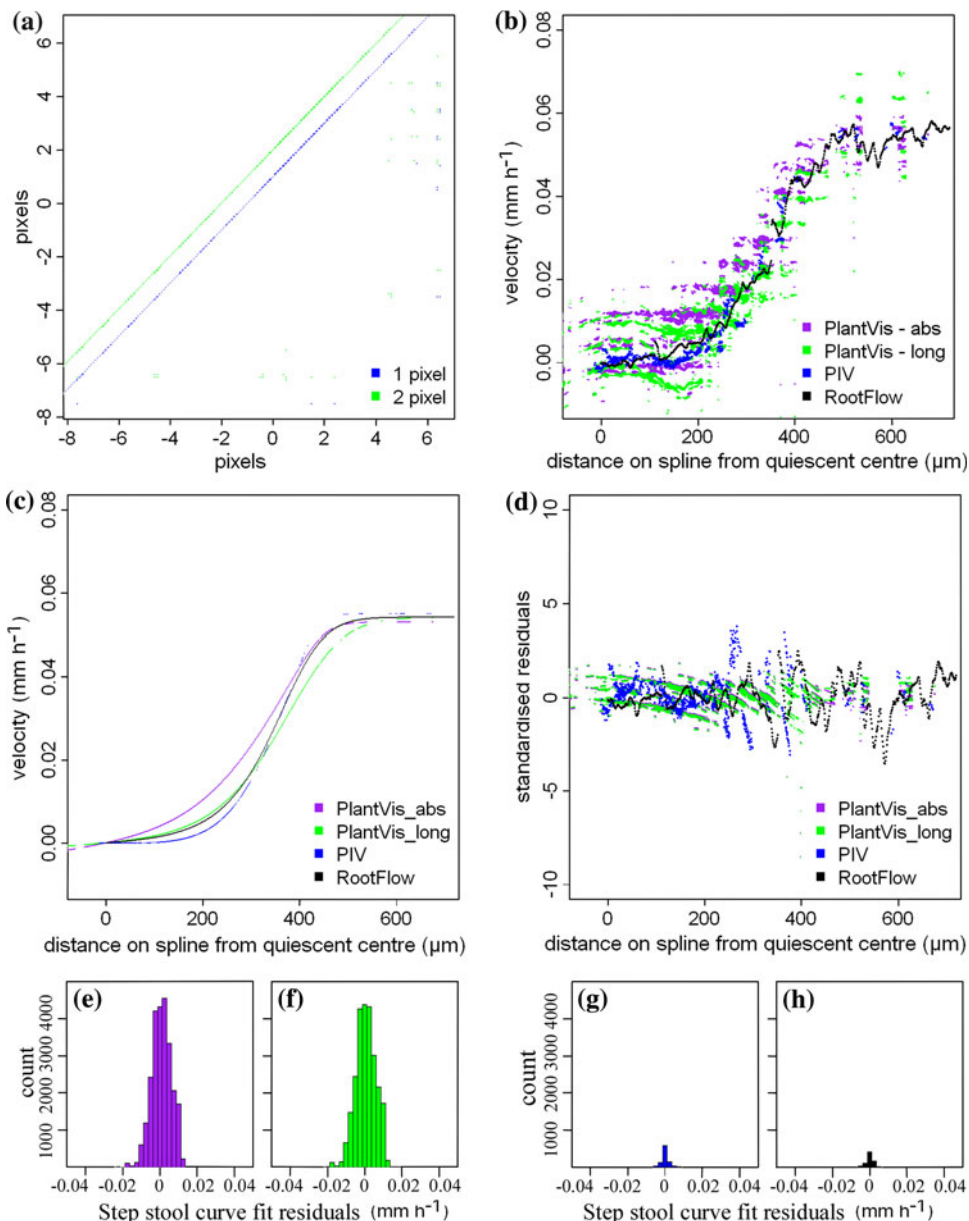
**Fig. 3** Analysis of the motion estimation output of *PlantVis* using *R* for a C24 LTI6b-EGFP primary root (8 DAG,  $\times 10$ ). CLSM root images overlaid with the central spline marker (green line in **a**), the quiescent centre marker (white  $x$  in **a**), or **b** the absolute velocity data points estimated and treated in this analysis. **c** Absolute, **d** longitudinal and **e** radial root growth (velocity) relative to the root growth axis (black)  $\pm$  standard deviation (grey). **f** Step-stool function (purple line) fitted to the root growth data (longitudinal velocity relative to the quiescent centre)



original data set. Figure 4a shows the vertical motion estimates from *PlantVis* for the artificial data sets plotted against the output of *PlantVis* for the unaltered data set. The data should have a slope of 1 and an intercept of 1 or 2 depending on the number of pixels added to the motion. The slopes of linear fits were  $0.994 \pm 0.000435\text{SE}$  ( $R^2 = 0.987$ ,  $n = 70,920$ ) and  $0.991 \pm 0.00748\text{SE}$  ( $R^2 = 0.962$ ,  $n = 69,385$ ) for the 1 and 2 pixels data sets, respectively. The intercepts were also as expected at  $1.008 \pm 0.00797\text{SE}$  and  $2.008 \pm 0.00137\text{SE}$  pixels for the 1 and 2 pixels data sets, respectively. Further 99.95 and 99.85% of pixels reported velocities exactly 1.0000 or 2.0000 pixels frame $^{-1}$  faster than the velocities reported for the original data set.

The velocity profile derived from the spatial distribution of motion estimated by *PlantVis* was also compared with velocity profiles generated by or calculated from two recent local-region based optical flow algorithms, *RootflowRT* (Jiang et al. 2003; van der Weele et al. 2003) and PIV (White et al. 2003; Bengough et al. 2010). *PlantVis* provided high confidence motion estimates for 67% of the root pixels (log likelihood threshold in *PlantVis* set to 60). In the case of *RootflowRT*, 1–7% of velocity data were obtained by the high confidence structure tensor algorithm, 45–57% by robust matching, which left 36–54% to be interpolated. The resulting velocity profiles and the fitted step-stool functions for a C24 *Arabidopsis* root (10 DAG)

**Fig. 4** Comparison of *PlantVis*, PIV and *RootflowRT*. **a** Motion estimates (pixels frame<sup>-1</sup>) for artificial data sets versus original data sets. Artificial data sets have 1 or 2 pixels frame<sup>-1</sup> added to the motion using *Leica* Microsoft software. **b** Velocity estimates from *PlantVis*, PIV and *RootflowRT* against distance from the quiescent centre. **c** Results of step-stool curve fit on velocity estimates for data sets plotted in **b** (values only plotted where data points exist). **d** Standardised residuals of step-stool curve fits against the distance from quiescent centre. **e, f, g, h** Count histograms of the residuals from the step-stool curve fit for *PlantVis* (absolute and longitudinal), PIV and *RootFlowRT*, respectively, showing the significantly higher number of data points exported by *PlantVis* compared with *RootFlowRT*



are shown in Fig. 4b and c, respectively. *PlantVis-R* recorded the highest rate of expansion in the division zone, followed by *RootflowRT* and PIV. Estimates of velocity in the expansion zone were similar although *PlantVis* suggested a slightly reduced expansion rate compared with the other two methods. *PlantVis-R* also recorded a more extended reduction in the rate of expansion at the end of the growth zone. Figure 4d shows the standardised residuals of each step-stool fit, plotted against the distance from the quiescent centre. Count histograms of the range of residuals for *PlantVis-R* (absolute and longitudinal velocities), PIV and *RootflowRT* step-stool curve fits are shown in Fig. 4e–h, respectively. The graphs demonstrate the significantly higher number of data points reported by *PlantVis* compared with *RootFlowRT* in this

example. While the standard deviation of the residuals of the Step stool curve fit for *PlantVis* was higher than both PIV and *RootflowRT* [0.0098 (absolute and longitudinal), 0.0019, 0.0020 respectively], the standard error of the residuals is of the same order of magnitude (6.2 E–05 (absolute and longitudinal), 6.2 E–05 and 7.3E–05, respectively). Spatial averaging is used to a greater extent in PIV and *RootFlowRT* and this will have the effect of reducing variance but increasing bias. Compared with the longitudinal velocity profile calculated using *PlantVis-R*, PIV and to a lesser extent *RootFlowRT* underestimated low velocity values (<0.03 mm h<sup>-1</sup>, closer to the quiescent centre). High velocity estimates (at the end of the elongation zone) were overestimated by PIV but were similar to those estimated by *RootFlowRT*.

### *PlantVis* : a flexible analysis tool

For each data point generated by *PlantVis*, the position in the image, the position in reference to the quiescent centre, the displacement in the image, and the velocity relative to the root spline are known. Thus, growth zones extracted using *PlantVis-R* analysis can be mapped directly onto the images used for the analysis to allow linking of profiles to specific cells. Figure 5 shows the *PlantVis-R* generated velocity data displayed in relation to the root structure and the root profile overlaid onto the CLSM root image from which it was generated. The vertical lines show the calculated beginning and end of elongation zones. Isolation of results by filtering for selected areas in the root image can also be applied in *R*. Examples of such areas are the root cap, epidermal and cortical cell files, and also individual cells and cell membranes (Fig. 6a–d). In bending roots, differential growth occurs across the root diameter (Fig. 6e–h). Selection of tissue on either side of the central axis of the root is a means for quantifying these growth processes. Velocity differs on either side of a bending root as shown in the velocity profile (Fig. 6g), which is accompanied by differences in the deduced EGR maximum and its position (Fig. 6h). The algorithm was designed and tested on images of roots expressing EGFP targeted to the plasma membrane, i.e. showing the outline of cells. However, its use of robust statistics and the fact that ambiguous (low certainty) motion estimates are not reported make it likely that it can yield useful motion estimates on other local grey value structures acquired by transmission imaging (CLSM, Fig. S1) or by digital imaging using light microscope optics. However, it has not been tested extensively on such images by the authors so researchers using the software on such images would need to assess empirically the accuracy of motion estimates.

#### Kinematic analysis of genetic variation in *A. thaliana* root growth in response to sucrose

To demonstrate the capabilities of the new root growth analysis procedure, extensive growth experiments were conducted involving over 160 data sets. Significant differences were found between the root lengths of two *A. thaliana* genotypes, C24 35S:LTI6b-EGFP and Col 35S:LTI6b-EGFP at 5, 8, and 11 days as measured using ImageJ on scanned images (10 replicates per treatment, data not shown). Root lengths were converted to growth rates over two time periods (5–8 days and 8–11 days) and compared with the tip root growth rates as measured by *PlantVis-R* (Fig. 7a). The velocity rates produced for the two genotypes were comparable between the two methods with C24 elongation rates accelerating over time and Col roots elongating faster, but at steady rates.

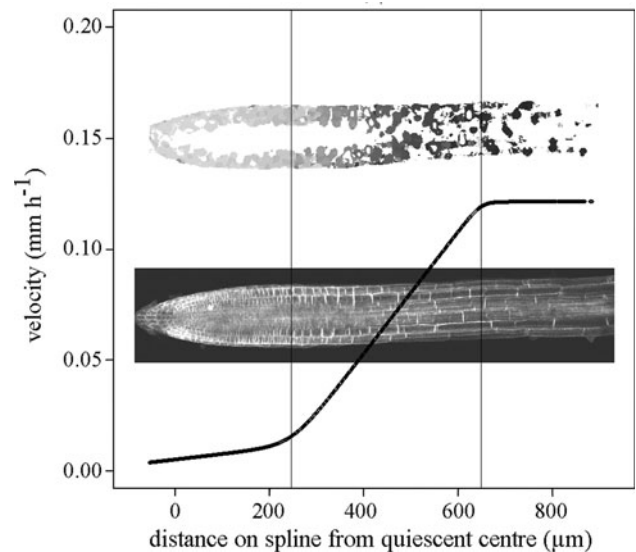
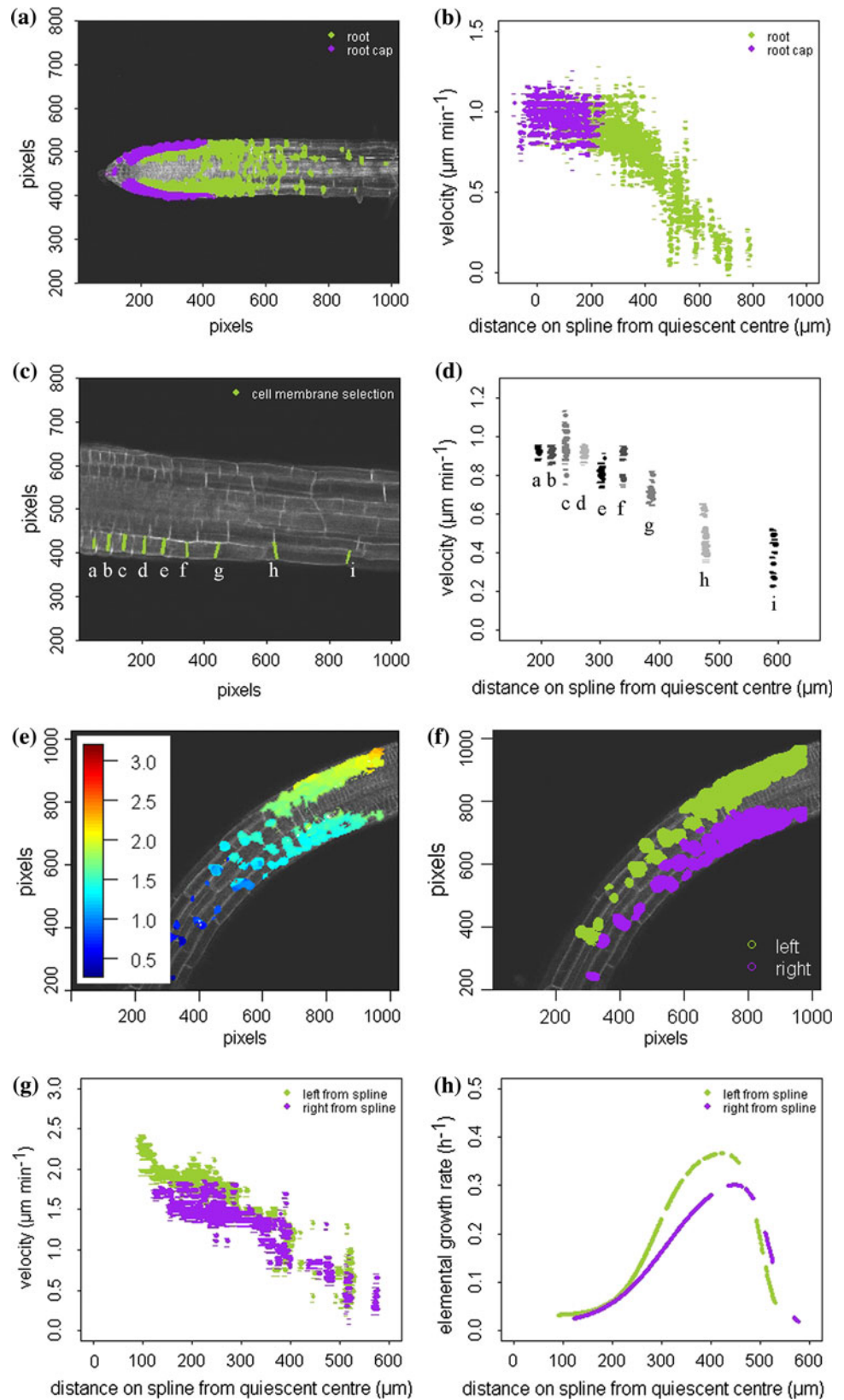


**Fig. 5** Step stool curve fit from *PlantVis* aligned to original root CLSM image and *PlantVis* estimated velocity data set image. Vertical lines represent the estimated beginning and end of the elongation zone

Parameters of the growth zones are detailed in Table 1. C24 roots grew on average between 1.15 and 1.30  $\mu\text{m min}^{-1}$  at 5 and 8 DAG, with velocity increasing to 2.25  $\mu\text{m min}^{-1}$  at 11 DAG, compared to Col roots which had a growth rate of 2.17–2.79  $\mu\text{m min}^{-1}$  (Table 1). The supplementary material contains videos demonstrating the difference in velocity between C24 and Col roots at 8 DAG (Fig. S2a and b, respectively). Root tip velocity increase in C24 roots was achieved by a significant increase in the length of the growth zone. The maximum EGR remained constant, which suggests that the roots grew faster potentially because of more cells expanding in the elongation zone. As the elongation zone became larger, the position of the maximum EGR shifted further back from the quiescent centre (Table 1). Col roots grew at steady-state with growth zones of equal lengths from 5 to 11 DAG. The maximum EGR was slightly lower at 11 DAG together with a small decrease in velocity.

Pearson's correlation coefficients were calculated for the growth parameters of individual plants (Tables S1 and S2). For C24, strong significant correlations were found between growth parameters, except for the length of the division zone and the maximum EGR. Col root growth parameters had less significant and weaker correlations, presumably because of steady-state growth resulting in a smaller range of values (Fig. S3). The reasons for the relatively poor correlation with division zone length and maximum EGR were studied in more detail. While the other growth parameters increased over time (to a greater or lesser extent) for individual roots,

**Fig. 6** Further potential analyses using *PlantVis-R*: growth analysis of selected root features. **a–d** *PlantVis-R* analysis results for an *A. thaliana* C24 LTI6b-EGFP primary root. Selection of a root cap and **c** cell membranes, using image analysis software (ImageJ) or the selection tool provided in *PlantVis*, and visualisation by *R* of the locations in the selected regions at which motion was estimated by *PlantVis* on the confocal image of the root. **b, d** Absolute velocity (points)  $\pm$  standard deviation (dashes) of selected root features. **e–h** *PlantVis-R* analysis results for a bending *A. thaliana* Col LTI6b-EGFP primary root. **e, f** Absolute velocity estimates and *left/right* points overlaid on original root CLSM image. **g, h** Absolute velocity (points)  $\pm$  standard deviation (dashes) and elemental growth rate profile along the root axis displayed selectively using filters for data *left* or *right* of the spline fitted to the root axis



the division zone length fluctuated and was sometimes smaller at 8 DAG than at 5 or 11 DAG. The same happened for the maximum EGR (Fig. S3).

The effect of 1% sucrose as growth medium supplement on C24 and Col root growth was investigated. C24 roots of an identical age showed no significant differences in root

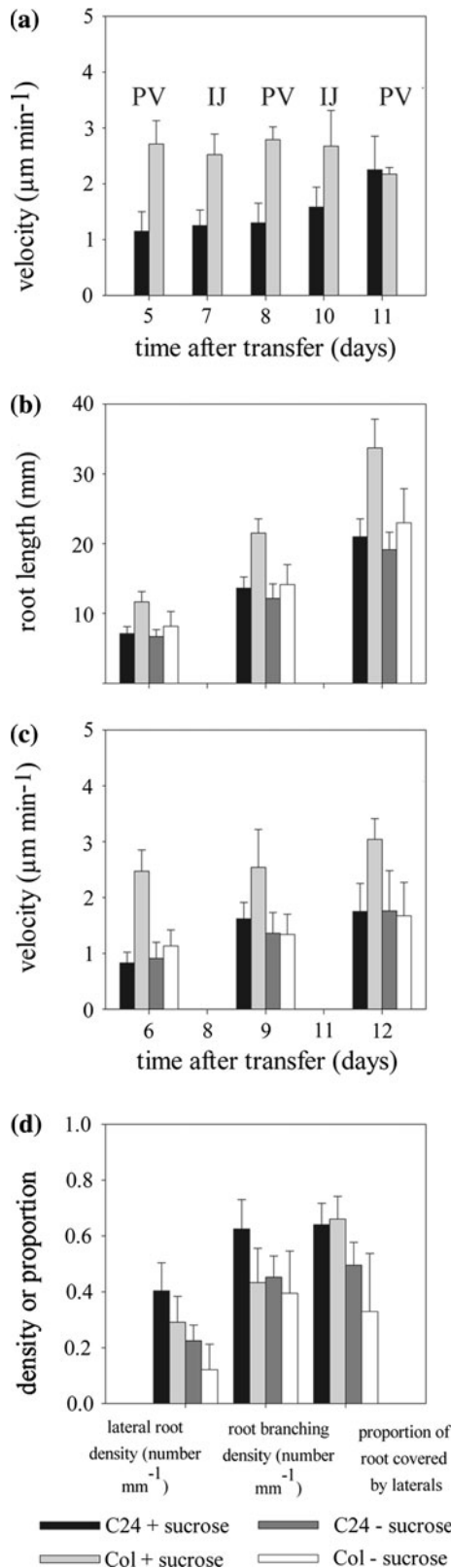


**Fig. 7** Root growth analysis of C24 and Col LTI6b-EGFP primary roots on media with (+) or without (-) 1% sucrose. **a** Root tip velocity (*IJ* denotes velocity calculated using ImageJ root measurements, *PV* denotes velocity measured using *PlantVis*). **b** Root length (measured using Image J). **c** Root tip velocity (*PlantVis*). **d** Lateral root density, root branching density and distribution of laterals for *A. thaliana* C24 and Col LTI6b-EGFP primary roots

growth, but at significantly slower rates on medium without sucrose resulting in roots that were significantly shorter (than with sucrose Col) and comparable in length to C24 roots (Fig. 7b, c). A summary of root growth profiles and parameters is shown in Fig. 8 and Table 2, respectively. Col growth parameters were comparable to C24 growth parameters for roots grown without sucrose, but showed significant differences when sucrose was present (Table 2). The maximum EGR and division zone length were not significantly different between treatments. However, Col roots in sucrose supplemented medium, exhibited more extensive elongation zones compared to Col roots growing on medium without sucrose. Fully expanded cells reached a length of  $114 \pm 26 \mu\text{m}$  in Col roots growing on medium with sucrose, while only reaching  $93 \pm 15 \mu\text{m}$  ( $P < 0.01$ ) on media without sucrose.

Significant differences in the number of lateral roots between media with or without sucrose were observed for both genotypes (Fig. 7d). Lateral root density (number of laterals per unit length of primary length) was approximately 50% smaller for roots growing on medium without sucrose. For C24, root branching density (number of laterals per lateral-producing portion of primary root length) was lower, with only a small reduction in the lateral-producing root length. Root branching density for Col was not significantly different between treatments, suggesting that a significantly smaller proportion of the root was producing laterals (50% reduction).

**Discussion**

The *PlantVis-R* combination has proven to be a very useful and flexible tool to analyse root growth responses of genotypes C24 and Col, including their responses to sucrose supplementation of growth media. In addition, using this software combination, highly dynamic root behaviour could be demonstrated and analysed.

**Root growth analysis with *PlantVis*—comparison with similar recent tools**

Recent growth analysis tools all claim high spatial and temporal resolution, compared to earlier work in the area of kinematic growth analysis (van der Weele et al. 2003; Bengough et al. 2010). Spatial and temporal resolution are,

length and growth parameters between treatments. C24 root growth on both treatments accelerated over the period of the experiment, whereas Col roots showed steady-state

**Table 1** Growth parameters determined using *PlantVis* and *R* for *A. thaliana* C24 and Col LTI6b-EGFP primary roots

Genotype	DAG	Root tip velocity ( $\mu\text{m min}^{-1}$ )	Elemental growth rate		Growth zone length ( $\mu\text{m}$ )	Division zone length ( $\mu\text{m}$ )	Elongation zone length ( $\mu\text{m}$ )
			Maximum ( $\% \text{ h}^{-1}$ )	Position ( $\mu\text{m}$ ) <sup>A</sup>			
C24	5	1.15 $\pm$ 0.35 <sup>a</sup>	30 $\pm$ 04 <sup>a</sup>	331 $\pm$ 54 <sup>a</sup>	423 $\pm$ 78 <sup>a</sup>	190 $\pm$ 36 <sup>a</sup>	233 $\pm$ 77 <sup>a</sup>
	8	1.30 $\pm$ 0.35 <sup>a</sup>	29 $\pm$ 11 <sup>a</sup>	334 $\pm$ 63 <sup>a</sup>	460 $\pm$ 89 <sup>a</sup>	205 $\pm$ 64 <sup>ab</sup>	256 $\pm$ 90 <sup>a</sup>
	11	2.25 $\pm$ 0.60 <sup>b</sup>	34 $\pm$ 04 <sup>a</sup>	464 $\pm$ 55 <sup>b</sup>	612 $\pm$ 98 <sup>b</sup>	253 $\pm$ 50 <sup>b</sup>	360 $\pm$ 76 <sup>b</sup>
		***	n.s.	***	***	*	**
Col	5	2.71 $\pm$ 0.42 <sup>a</sup>	37 $\pm$ 06 <sup>a</sup>	463 $\pm$ 51 <sup>a</sup>	608 $\pm$ 59 <sup>a</sup>	240 $\pm$ 50 <sup>a</sup>	366 $\pm$ 69 <sup>a</sup>
	8	2.79 $\pm$ 0.23 <sup>a</sup>	37 $\pm$ 03 <sup>ab</sup>	489 $\pm$ 42 <sup>a</sup>	628 $\pm$ 22 <sup>a</sup>	269 $\pm$ 47 <sup>a</sup>	359 $\pm$ 41 <sup>a</sup>
	11	2.17 $\pm$ 0.12 <sup>a</sup>	26 $\pm$ 01 <sup>b</sup>	560 $\pm$ 69 <sup>a</sup>	701 $\pm$ 72 <sup>a</sup>	307 $\pm$ 30 <sup>a</sup>	394 $\pm$ 51 <sup>a</sup>
		n.s.	*	n.s.	n.s.	n.s.	n.s.

Data are averages ( $\pm$  standard deviation) of ten replicate primary roots

DAG days after germination

For each genotype, data in the same column followed by the same letter are not significantly different according to the Tukey-test. \*, \*\*, \*\*\*, n.s. indicate that the differences between DAG are significant at  $P < 0.05$ , 0.01, 0.001 or not, respectively

<sup>A</sup> Position as distance from the quiescent centre

however, dependent on the imaging system and as such, the purpose of the experiment. Imaging over longer time periods (hours) is required to study the impact of environmental changes on whole-organ root growth behaviour and, as such, digital cameras are often used to capture roots growing in controlled environments (Vollsnæs et al. 2010). This results in a (moderate) loss of spatial and temporal resolution, but allows for the analysis over longer time periods (French et al. 2009) or the bigger root systems of crop plants, e.g. *Zea mays* or *Phaseolus vulgaris* (Walter et al. 2002; Basu et al. 2007). On the other hand, *PlantVis* (Roberts et al. 2010) and *RootflowRT* (van der Weele et al. 2003) are tools designed for much smaller displacements between frames in an imaging environment not ideal for longer periods of (semi-) continuous imaging. *PlantVis* can, however, be applied to longer sequences generated by discontinuous imaging. Both *PlantVis-R* and *RootflowRT* provide higher displacement accuracy, which is required for detailed analysis of spatially and temporally variable growth rates.

All recent (semi-)automated digital image processing tools deliver relatively good spatial and temporal resolution, but are limited by the information present in images of root surfaces. Two algorithms for the generation of DVFs that are currently in use for similar applications are based on local grey value structures in root surface images. The structure tensor algorithm (Bigün and Granlund 1987) aims at providing a dense DVF by attempting velocity estimation at each pixel. Pixels with a high probability of being unreliable are rejected, which results in an unevenly filled DVF (5–30% of root pixels contain valuable motion information). Normalised convolution is then applied to generate a dense interpolated DVF (Schmudt et al. 1998;

Walter et al. 2002; van der Weele et al. 2003; Chavarría-Krauser et al. 2008). Robust matching (Black and Anandan 1996) is added in the *RootflowRT* algorithm to improve the density of confident motion information, but interpolation is still required for 40–50% of root pixels (Jiang et al. 2003; van der Weele et al. 2003). Basu et al. (2007) have used graphite particles to increase patterning in images of root surfaces, hence improving the certainty of matches between local patches. Their patch matching algorithm is based on a highest correlation coefficient search, with a measure of confidence, but patches of local structure are tracked only for a limited number (10–15) of user-chosen points along the root, resulting in a coarsely filled DVF. In contrast, *PlantVis* delivers a DVF specifically for root features and without interpolation (generally for >60% of root feature pixels).

Significant differences between *PlantVis* or PIV (Bengough et al. 2010) and *RootflowRT* (van der Weele et al. 2003) are the ability to analyse fluorescent images captured by CLSM and the analysis of growth in bending roots. Analysis of the same data set using *PlantVis*, PIV and *RootFlowRT* gave slightly different positions and rate of expansion. The curve generated by *RootFlowRT* fell between the absolute and longitudinal velocity (with the velocities being nearer to the longitudinal velocity in the transition zone, and nearer to the absolute velocity in towards the end of the elongation zone) suggesting that this algorithm is not taking into account the radial motion present in this data set (*RootFlowRT* is designed for straight growing roots). PIV produced a similar curve to *RootFlowRT* in the middle of the elongation zone, but underestimated the velocities in the division zone and overestimated velocities towards the end of the elongation zone

**Fig. 8** Average velocity and elemental growth rate profiles of *A. thaliana* C24 and Col LTI6b-EGFP primary roots at 6, 9 and 12 DAG on media with or without 1% sucrose. **a, c** *R* was applied on motion estimated by *PlantVis* to obtain velocity profiles and fit the step-stool function. **b, d** The elemental growth rate profile is obtained as the first derivative of the step-stool function. **a, b** C24. **c, d** Col

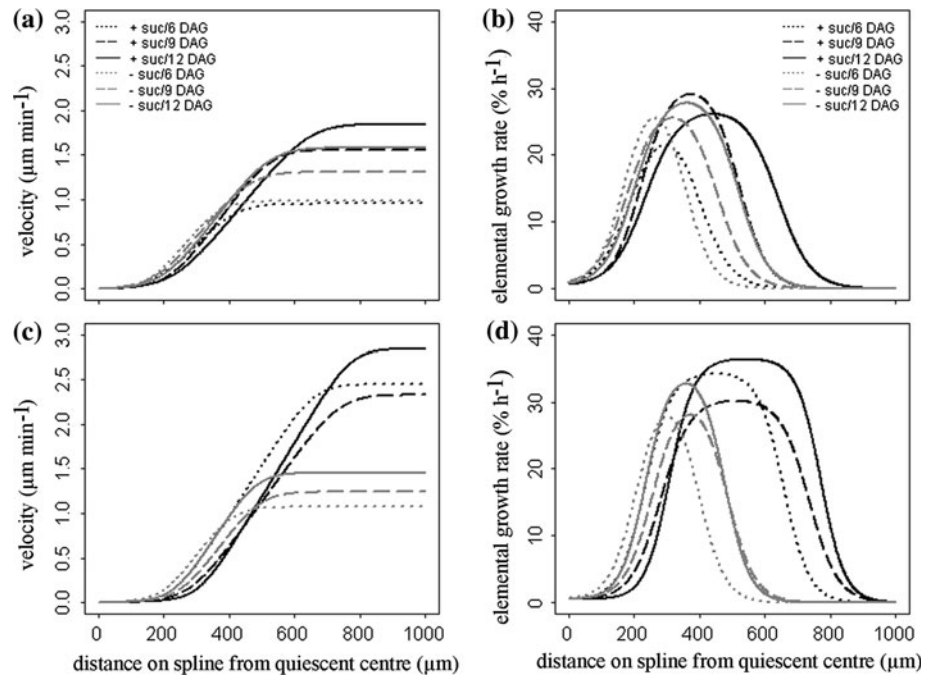


**Table 2** Growth parameters determined using *PlantVis* and *R* for *A. thaliana* C24 and Col LTI6b-EGFP primary roots growing with or without supplemented sucrose

Genotype/ treatment	DAG	Root tip velocity ( $\mu\text{m min}^{-1}$ )	Elemental growth rate		Growth zone length ( $\mu\text{m}$ )	Division zone length ( $\mu\text{m}$ )	Elongation zone length ( $\mu\text{m}$ )
			Maximum ( $\% \text{h}^{-1}$ )	Position ( $\mu\text{m}$ ) <sup>A</sup>			
C24/+suc	6	$0.83 \pm 0.19^a$	$22 \pm 2^a$	$304 \pm 044^{ac}$	$398 \pm 061^a$	$193 \pm 24^{ab}$	$204 \pm 061^a$
	9	$1.62 \pm 0.29^b$	$29 \pm 3^a$	$391 \pm 045^{bc}$	$522 \pm 025^{ab}$	$223 \pm 35^{ab}$	$288 \pm 036^{ab}$
	12	$1.75 \pm 0.50^b$	$26 \pm 6^a$	$474 \pm 084^b$	$642 \pm 104^b$	$235 \pm 48^b$	$411 \pm 087^b$
C24/-suc	6	$0.91 \pm 0.29^a$	$26 \pm 3^a$	$267 \pm 064^a$	$354 \pm 076^a$	$172 \pm 36^a$	$181 \pm 064^a$
	9	$1.36 \pm 0.37^{ab}$	$26 \pm 2^a$	$322 \pm 023^{ab}$	$455 \pm 069^{ab}$	$181 \pm 17^a$	$298 \pm 080^{ab}$
	12	$1.76 \pm 0.72^b$	$28 \pm 7^a$	$356 \pm 107^{ab}$	$520 \pm 190^{ab}$	$201 \pm 44^{ab}$	$318 \pm 155^{ab}$
		***	n.s.	**	**	*	**
Col/+suc	6	$2.47 \pm 0.38^a$	$34 \pm 7^a$	$503 \pm 69^a$	$658 \pm 95^a$	$235 \pm 60^{ac}$	$423 \pm 098^a$
	9	$2.54 \pm 0.68^a$	$30 \pm 5^a$	$558 \pm 91^{ab}$	$736 \pm 94^a$	$282 \pm 44^{ab}$	$456 \pm 067^a$
	12	$3.04 \pm 0.37^a$	$36 \pm 5^a$	$631 \pm 60^b$	$772 \pm 81^a$	$309 \pm 38^b$	$474 \pm 103^a$
Col/-suc	6	$1.13 \pm 0.29^b$	$28 \pm 8^a$	$312 \pm 59^c$	$397 \pm 67^b$	$208 \pm 52^c$	$189 \pm 051^b$
	9	$1.34 \pm 0.36^b$	$28 \pm 7^a$	$378 \pm 70^c$	$486 \pm 76^b$	$257 \pm 64^{bc}$	$229 \pm 019^b$
	12	$1.67 \pm 0.60^b$	$33 \pm 6^a$	$375 \pm 71^c$	$479 \pm 99^b$	$236 \pm 41^{bc}$	$243 \pm 074^b$
		****	n.s.	***	****	*	****

Data are averages ( $\pm$  standard deviation) of ten replicate primary roots  
DAG days after germination

For each genotype, data in the same column followed by the same letter are not significantly different according to the Tukey-test. \*, \*\*, \*\*\*, n.s. indicate that the differences between DAG and treatments are significant at  $P < 0.05, 0.01, 0.001$  or not, respectively

<sup>A</sup> Position as distance from the quiescent centre

compared with *PlantVis*. Bengough et al. (2010) showed that the effectiveness of PIV tracking was reduced in areas of fast expansion, rather than due to rigid translation, the combination of the cell expansion in preparation for division and the lateral movement due to unequal expansion

may, therefore, be the potential cause of the discrepancy between the curves in the division zone and the later elongation zone.

CLSM imaging can capture local structures in the images corresponding to meaningful root features, such as

cell membranes and vertices. Recently, PIV was reported as a technique useful for analysis of root cell expansion (Bengough et al. 2010). In comparison, *PlantVis* examines all pixels in the images, but reports only on pixels to which it can confidently assign displacement estimates based on the log likelihood threshold set. Moreover, it gives a measure of uncertainty at each such pixel, enabling automated selection of data from large data sets of motion estimates, whereas PIV included no estimate of confidence. Displacement and uncertainty are reported on a per pixel basis rather than as averages across the root diameter, which means that velocity can be retrieved for specific root features, like a cortical cell file along the root or a small area of pixels making up a cell membrane. This is in contrast to many other root tracking methods where the variance reported originates from averaging of velocities across the root diameter or across time periods. *Plantvis* does, however, report a small proportion of data points that have high residuals when the step stool function is fitted. These appear as scatter on the graphs shown in Fig. 3c–f, for example. A contributory source of these data points is biological membrane movement and detaching cells from the root cap periphery. This issue is not exclusive to *PlantVis*; a particular extreme effect of this can be found in the comparison of 35S:LTI-EGFP lines with 35S:GFP expressing lines, where the movement of the GFP-labelled endoplasmic reticulum was shown to significantly affect the results achieved when using PIV (Bengough et al. 2010). Thus, *PlantVis* extends PIV capabilities by allowing the user to set data confidence thresholds, both at the stage of motion estimation, and using the certainty value output by *PlantVis* during data processing in R.

Genotype-dependent responses to exogenous carbon supply can overcome root growth limitations imposed by endogenous carbon assimilation and transport

A comparison of reported *A. thaliana* primary root tip velocity, as measured by different image analysis procedures, is problematic due to differing experimental methodologies, including genotype, seedling age, day/night regimes (continuous light or 12–16 h day length), temperature conditions (19–25°C) and growth media (type of macro- and micro-elements, vitamins and sucrose supplements ranging from no sucrose to 0.5–3%). Growth rates of C24 reported here range from 0.91 to 1.76  $\mu\text{m min}^{-1}$  (without sucrose, 6–12 days old seedlings, 16 h day) to 0.83–2.25  $\mu\text{m min}^{-1}$  (with sucrose, 6–12 days old seedlings, 16 h day), in comparison with 1.65  $\mu\text{m min}^{-1}$  measured by Beemster et al. (2002; with sucrose 6–10 days old seedlings, continuous light). Growth rates of Col reported range from 1.68  $\mu\text{m min}^{-1}$  (Chavarria-Krauser et al. 2008, without sucrose, 9 day old seedlings,

12 h day), up to 4.01  $\mu\text{m min}^{-1}$  (Beemster and Baskin 1998; Mullen et al. 1998; Miller et al. 2007; with or without sucrose, 3–6 days old seedlings, continuous light) and up to more than 6  $\mu\text{m min}^{-1}$  (Beemster and Baskin 1998; van der Weele et al. 2003, with or without sucrose, 9–10 days old seedlings, continuous light). These are comparable with the growth rates measured here, of 2.17–3.04  $\mu\text{m min}^{-1}$  or 1.13–1.67 for Col with or without sucrose, respectively (6–12 days old seedlings, 16 h day).

The EGR of 22–37%  $\text{h}^{-1}$  (16 h day), is similar in proportion to the reported EGR of 25–37%  $\text{h}^{-1}$  (Chavarria-Krauser et al. 2008, 12 h day) but lower than those reported under continuous light (35–50%  $\text{h}^{-1}$ , Beemster and Baskin 1998; Mullen et al. 1998; Beemster et al. 2002; van der Weele et al. 2003). Under these conditions C24 cells expand to a mature length of  $94 \pm 2 \mu\text{m}$ , compared to  $171 \pm 12 \mu\text{m}$  for Col producing a longer elongation zone in Col (Beemster et al. 2002).

C24 growth rates increased gradually over the period of 5–12 days regardless of the presence of sucrose, suggesting that C24 is not capable of utilising exogenously supplied sucrose for primary root elongation. Constant light conditions do have a positive effect on root growth rate (as discussed above) suggesting, that under carbon-limited conditions C24 root growth is adjusted to the endogenous supply of carbon (assimilation and transport), which increases as the rosette develops. In case of Col, root growth rate was affected by sucrose deprivation in the growth medium, as roots failed to acquire a constant high growth rate within 5 DAG. This was caused by a reduction in the extent of the elongation zone, while the maximum EGR remained equal and division zones were of similar size. The elongation zone was smaller because individual cells left the elongation zone at a shorter length (by approximately 20  $\mu\text{m}$ ). Therefore, Col root growth is also adjusted to the endogenous supply of carbon under carbon-limited conditions, while in contrast with C24, Col roots do appear to assimilate exogenously supplied sucrose. This supports the finding of Freixes et al. (2002) who measured 50% slower growth rates under low light conditions, without sucrose, but equally high rates whether light intensities were high or low, in the presence of sucrose in the growth medium.

Lateral root development is affected by an exogenous supply of carbon

While sucrose did not affect C24 primary root growth parameters, it did have a pronounced effect on lateral root development of both C24 and Col. Without exogenously supplied sucrose, lateral root density was 50% smaller. C24 produced fewer laterals, which meant that the endogenous carbon supply was preferably allocated to primary root

growth, without affecting the timing of lateral root emergence during development. In Col, the addition of sucrose in the growth medium made laterals emerge closer to the quiescent centre, but did not initiate more lateral roots. Under endogenous carbon conditions, laterals emerged later during development. Potentially, auxin transport—or the local action of auxin along the root axis—is inherently different between both genotypes and could be altered by the addition of sucrose in the case of Col (Casimiro et al. 2001). More detailed research on the effects of sucrose on root system development is warranted.

Increased growth rates can be achieved by enlarged division zone but seemingly not as a continuous process

In the current experiments, with a 16 h day length, C24 root growth rate increased over time, mainly between 8 and 10 DAG, because of a lengthening growth zone, while the average maximum elongation rate remained constant. Beemster and Baskin (1998) concluded that these increased growth rates and lengthening growth zones are achieved by a higher flux of cells from the division zone into the elongation zone, which in itself is due to an increased number of dividing cells. This means that, as the division zone develops, cells continue dividing for longer periods. Dello Ioio et al. (2007) have recently provided evidence for an auxin-antagonistic role for cytokinin in the regulation of division zone size, such that the division zone size increases after germination until a maximum size is reached and root growth rate becomes constant. In their experiments, under conditions similar to the experiments described here, this occurred at 5 DAG for Col roots, which corresponds to our observations of constant growth rates at 5 DAG and beyond. However, in our experiments, using Col there was no strong correlation between division zone size and other growth parameters, such as velocity and maximum EGR. We found that, at the individual root level, division zone size can fluctuate over time, together with fluctuations in the maximum EGR. These observations could only be recorded with a tool measuring kinematic changes over short intervals.

Determination of the division zone - elongation zone boundary

The root growth zone is often divided into the division, elongation and, differentiation zones (Beemster and Baskin 1998; Berger et al. 1998; Birnbaum et al. 2003). Various alternative methods have been used to track cell division to determine the end of the division zone including cell size (Beemster et al. 2002), cell flux rates (Beemster and Baskin

1998), cellular characteristics (Birnbaum et al. 2003) and cell developmental status as indicated by GFP marker lines (Dello Ioio et al. 2007). The cell cycle in *Arabidopsis* root takes in the region of 18 h to complete, thus it is not possible within the data sets acquired here to determine the boundary between the division zone and elongation zone by tracking cell division alone. Beemster and Baskin (1998) measured cell production rates in *Arabidopsis* roots, and compared them with the spatial profile of expansion. They suggested that cell division activity may continue up to the maximum strain rate, and thus cell division was occurring beyond the point at which cells were starting to expand. Further using cell characteristics and transgenic lines, Verbelen et al. (2006) also suggested there may be a more complicated transition between division and elongation zones, suggesting that there were four zones within the growth zone (division, transition, fast elongation, and growth termination). The velocity profiles obtained by *PlantVis-R* are based on local displacement differences, and showed a smooth rather than abrupt transition between the near constant displacements in the region closest to the quiescent centre, i.e. the division zone, and the region with large displacement differences, i.e. the elongation zone in many cases. This was confirmed by detailed examination of how the root growth profiles mapped onto images of the root tip (e.g. Fig. 5). In this paper, the inflection point of the velocity profile was used to mark the boundary between the division zone and the elongation zone and is thus situated within the transition zone. Using a combination of *PlantVis* to produce detailed motion analysis of roots and the combined ability to visualise cell developmental status by means of fluorescent marker lines (e.g. Dello Ioio et al. 2007), it will now be possible to investigate the link between velocity rates and cell developmental status in more detail.

*PlantVis* in combination with R and ImageJ is a very valuable tool in physiological studies of (differential) root growth processes at the root, tissue and cell level. In combination with a second fluorescently tagged protein in an individual plant, there is the potential to link both expression analysis or protein location studies with their effect on cell expansion and corresponding effects on root growth. Although this paper describes kinematic growth analysis, for which scripts have been developed in R, additional analyses, such as the determination of cell number and size for the calculation of cell flux and production rate may be performed simultaneously (Beemster and Baskin 1998). *PlantVis* therefore has considerable potential for use in studies of root responses to the local environment.

The *PlantVis* software and R-scripts are available for academic non-commercial research from the corresponding author (see also <http://www.phytocomp.org.uk>).

**Acknowledgments** Prof. Jim Haseloff (Cambridge University) for the kind donation of *A. thaliana*. D. White (University of Western Australia) for access to the Cambridge University PIV code. This work was funded by the Biotechnology and Biological Sciences Research Council (BBSRC), UK. SCRI receives grant-in-aid from the Scottish Government Rural and Environmental Research and Analysis Directorate (SG-RERAD). Dr. Kath Wright, Dr. Lionel Dupuy and Prof. Philip White for helpful comments on this manuscript.

## References

- Barbier de Reuille P, Bohn-Courseau I, Godin C, Traas J (2005) A protocol to analyse cellular dynamics during plant development. *Plant J* 44:1045–1053
- Basu P, Pal A, Lynch JP, Brown KM (2007) A novel image-analysis technique for kinematic study of growth and curvature. *Plant Physiol* 145:305–316
- Beemster GTS, Baskin TI (1998) Analysis of cell division and elongation underlying the developmental acceleration of root growth in *Arabidopsis thaliana*. *Plant Physiol* 116:1515–1526
- Beemster GTS, Baskin TI (2000) *STUNTED PLANT 1* mediates effects of cytokinin, but not of auxin, on cell division and expansion in the root of *Arabidopsis*. *Plant Physiol* 124:1718–1727
- Beemster GTS, De Vusser K, De Tavernier E, De Bock K, Inze D (2002) Variation in growth rate between *Arabidopsis* genotypes is correlated with cell division and A-type cyclin-dependent kinase activity. *Plant Physiol* 129:854–864
- Bengough AG, Hans J, Bransby MF, Valentine TA (2010) PIV as a method for quantifying root cell growth and particle displacement in confocal images. *Microsc Res Tech* 73:27–36
- Berger F, Haseloff J, Schiefelbein J, Dolan L (1998) Positional information in root epidermis is defined during embryogenesis and acts in domains with strict boundaries. *Curr Biol* 8:421–430
- Bigiñ J, Granlund GH (1987) Optimal orientation detection of linear symmetry. In: Proceedings of the first international conference on computer vision, London, 8–11 June 1987. IEEE Computer Society Press, Washington, DC, pp 433–438
- Birnbaum K, Shasha DE, Wang JY, Jung JW, Lambert GM, Galbraith DW, Benfey PN (2003) A gene expression map of the *Arabidopsis* root. *Science* 302:1956–1960
- Black MJ, Anandan P (1996) The robust estimation of multiple motions: parametric and piecewise-smooth flow-fields. *Comput Vis Image Underst* 63:75–104
- Campilho A, Garcia B, van der Toorn H, van Wijk H, Campilho A, Scheres B (2006) Time-lapse analysis of stem-cell divisions in the *Arabidopsis thaliana* root meristem. *Plant J* 48:619–627
- Casimiro I, Marchant A, Bhalerao RP, Beeckman T, Dhooge S, Swarup R, Graham N, Inze D, Sandberg G, Casero PJ, Bennett M (2001) Auxin transport promotes *Arabidopsis* lateral root initiation. *Plant Cell* 13:843–852
- Chavarria-Krauser A, Nagel KA, Palme K, Schurr U, Walter A, Scharr H (2008) Spatio-temporal quantification of differential growth processes in root growth zones based on a novel combination of image sequence processing and refined concepts describing curvature production. *New Phytol* 177:811–821
- Cutler SR, Ehrhardt DW, Griffiths JS, Somerville CR (2000) Random GFP:cDNA fusions enable visualization of subcellular structures in cells of *Arabidopsis* at a high frequency. *Proc Natl Acad Sci USA* 97:3718–3723
- De Veylder L, Beemster GTS, Beeckman T, Inze D (2001) CKS1At overexpression in *Arabidopsis thaliana* inhibits growth by reducing meristem size and inhibiting cell-cycle progression. *Plant J* 25:617–626
- Dello Ioio R, Linhares FS, Scacchi E, Casamitjana-Martinez E, Heidstra R, Costantino P, Sabatini S (2007) Cytokinins determine *Arabidopsis* root-meristem size by controlling cell differentiation. *Curr Biol* 17:678–682
- Freixes S, Thibaud MC, Tardieu F, Muller B (2002) Root elongation and branching is related to local hexose concentration in *Arabidopsis thaliana* seedlings. *Plant Cell Environ* 25:1357–1366
- French A, Ubeda-Tomás S, Holman TJ, Bennett MJ, Pridmore T (2009) High-throughput quantification of root growth using a novel image-analysis tool. *Plant Physiol* 150:1784–1795
- Hammond JP, White PJ (2008) Sucrose transport in the phloem: integrating root responses to phosphorus starvation. *J Exp Bot* 59:93–109
- Hauser MT, Bauer E (2000) Histochemical analysis of root meristem activity in *Arabidopsis thaliana* using a cyclin: GUS (beta-glucuronidase) marker line. *Plant Soil* 226:1–10
- Hermans C, Hammond JP, White PJ, Verbruggen N (2006) How do plants respond to nutrient shortage by biomass allocation? *Trends Plant Sci* 11:611–617
- Jiang HS, Palaniappan K, Baskin TI (2003) A combined matching and tensor method to obtain high fidelity velocity fields from image sequences of the non-rigid motion of the growth of a plant root. In: Hamza MH (ed) IASTED international conference on biomedical engineering, BioMED 2003. ACTA Press, Calgary, Canada, 386–010, pp 159–165
- Kurup S, Runions J, Kohler U, Laplaze L, Hodge S, Haseloff J (2005) Marking cell lineages in living tissues. *Plant J* 42:444–453
- MacGregor DR, Deak KI, Ingram PA, Malamy JE (2008) Root system architecture in *Arabidopsis* grown in culture is regulated by sucrose uptake in the aerial tissues. *Plant Cell* 20:2643–2660
- Miller ND, Parks BM, Spalding EP (2007) Computer-vision analysis of seedling responses to light and gravity. *Plant J* 52:374–381
- Mullen JL, Ishikawa H, Evans ML (1998) Analysis of changes in relative elemental growth rate patterns in the elongation zone of *Arabidopsis* roots upon gravistimulation. *Planta* 206:598–603
- Peters WS, Baskin TI (2006) Tailor-made composite functions as tools in model choice: the case of sigmoidal vs bi-linear growth profiles. *Plant Methods* 2:11
- Reddy GV, Gordon SP, Meyerowitz EM (2007) Unravelling developmental dynamics: transient intervention and live imaging in plants. *Nat Rev Mol Cell Biol* 8:491–501
- Roberts TJ, McKenna SJ, Du CJ, Wuyts N, Valentine TA, Bengough AG (2010) Estimating the motion of plant root cells from in vivo confocal laser scanning microscopy images. *Mach Vis Appl* 21:921–939
- Rolland F, Moore B, Sheen J (2002) Sugar sensing and signaling in plants. *Plant Cell* 14:S185–S205
- Schmundt D, Stitt M, Jähne B, Schurr U (1998) Quantitative analysis of the local rates of growth of dicot leaves at a high temporal and spatial resolution, using image sequence analysis. *Plant J* 16:505–514
- Shimizu M, Okutomi M (2005) Sub-pixel estimation error cancellation on area-based matching. *Int J Comput Vision* 63:207–224
- Teale WD, Paponov IA, Ditengou F, Palme K (2005) Auxin and the developing root of *Arabidopsis thaliana*. *Physiol Plant* 123:130–138
- van der Weele CM, Jiang HS, Palaniappan KK, Ivanov VB, Palaniappan K, Baskin TI (2003) A new algorithm for computational image analysis of deformable motion at high spatial and temporal resolution applied to root growth. Roughly uniform elongation in the meristem and also, after an abrupt acceleration, in the elongation zone. *Plant Physiol* 132:1138–1148

- Verbelen JP, De Cnodder T, Le J, Vissenberg K, Baluska F (2006) The root apex of *Arabidopsis thaliana* consists of four distinct zones of growth activities. *Plant Signal Behav* 1:296–304
- Vollsnes AV, Futsaether C, Bengough AG (2010) Quantifying rhizosphere particle movement around mutant maize roots using timelapse imaging and particle image velocimetry. *Eur J Soil Sci* 61:926–939
- Walter A, Spies H, Terjung S, Kusters R, Kirchgessner N, Schurr U (2002) Spatio-temporal dynamics of expansion growth in roots: automatic quantification of diurnal course and temperature response by digital image sequence processing. *J Exp Bot* 53:689–698
- White DJ, Take WA, Bolton MD (2003) Soil deformation measurement using particle image velocimetry (PIV) and photogrammetry. *Geotechnique* 53:619–631